# Gas-phase synthesis of non-agglomerated nanoparticles by fast gasdynamic heating and cooling

**A. Grzona[1], A. Weiß[1], H. Olivier[1], T. Gawehn[2], A. Gülhan[2], N. Al-Hasan[3], G.H. Schnerr[3], A. Abdali[4], M. Luong[4], H. Wiggers[4], C. Schulz[4], J. Chun[5], B. Weigand[5], T. Winnemöller[6], W. Schröder[6], T. Rakel[7], K. Schaber[7], V. Goertz[8], H. Nirschl[8], A. Maisels[9], W. Leibold[9], and M. Dannehl[9]**

[1] *Shock Wave Laboratory, RWTH Aachen University, 52056 Aachen, Germany*
[2] *German Aerospace Center, Wind Tunnel Department, Linder Höhe, 51147 Köln, Germany*
[3] *Lehrstuhl für Fluidmechanik - Fachgebiet Gasdynamik, TU München, Boltzmannstr. 15, 85748 Garching, Germany*
[4] *IVG, University of Duisburg-Essen, 47048 Duisburg, Germany*
[5] *Institute of Aerospace Thermodynamics, Universität Stuttgart, Pfaffenwaldring 31, 70569 Stuttgart, Germany*
[6] *Institute of Aerodynamics, RWTH Aachen University, 52056 Aachen, Germany*
[7] *Institut für Technische Thermodynamik und Kältetechnik, Universität Karlsruhe, Engler-Bunte-Ring 21, 76131 Karlsruhe, Germany*
[8] *Institut für Mechanische Verfahrenstechnik und Mechanik, Universität Karlsruhe, Straße am Forum 8, 76131 Karlsruhe, Germany*
[9] *Degussa GmbH, Rodenbacher Chaussee 4, 63457 Hanau, Germany*

## 1 Introduction

Gas-phase synthesized nanoparticles are broadly used in industry, science and measurement technology. Today flame synthesis and hot-wall synthesis are the most widely used methods for industrial production with an annual volume of several million tons. Remarkable is, that the morphology of the synthesized particles does not vary significantly. Most of them are aggregates with a fractal dimension of 1.8 - 1.9 and a geometric standard deviation of the size distribution in the range of 1.5 - 1.7. Former studies indicate that a homogeneous flow field and high heating and quenching rates are of major importance to achieve narrow size distribution and low aggregation. [1]

Therefore, in the frame of the project "Gasdynamically induced nano-particles" supported by the Deutsche Forschungsgemeinschaft (DFG) a novel method for the production of oxide nanoparticles from gas-phase precursors in a shock-wave flow reactor is

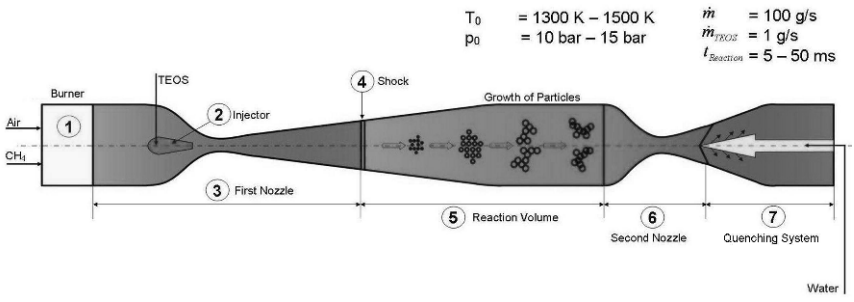


**Fig. 1.** Principle of operation

presented in this paper. In contrast to conventional methods the gas mixture is instantaneously heated by a stationary shock wave of an overexpanded supersonic nozzle flow. An overview of the principle of operation is given in Fig. 1. Following the injection of the precursor gas (2) the flow accelerates to supersonic flow speed and the reaction is initiated by shock wave heating (4). Chemical processes lead to the generation and growth of nanoparticles in the reaction chamber (5). After an adjustable reaction time depending on the gas velocity and the reactor length, the reaction is terminated due to rapid expansion and, therefore, cooling of the gas in a convergent-divergent nozzle flow (6). The total enthalpy of the flow is finally reduced by injecting water in a quenching system downstream of the second nozzle exit (7). This work is focused on numerical and experimental investigations of the underlying fluid-dynamic and chemical-kinetic requirements, to compose a design strategy of a pilot facility.

## 2 Numerical Simulation and Comparison with Experiment

The basic layout of the first nozzle (3) is defined by the pre-shock Mach number, the design mass flow rate and the distance from the injection location of the precursor to the shock location. The minimum of this distance follows from the required mixing length of the precursor with the air. The maximum allowable length is prescribed by the ignition delay of the precursor under the given thermal conditions. The throat area of the second nozzle (6) has to be matched, according to the change of the critical density and total temperature as a result of the shock losses, the viscous losses, the reactive heat addition and the wall cooling. In Fig. 2a the static temperature distribution along the axis of the facility is depicted as result of a 3-D numerical simulation. The turbulent simulation (SST-model) includes the effects of the reactive heat addition, wall cooling and temperature dependent fluid properties. In this case the reactive heat is modeled by a prescribed heat addition. The timescales of the shock induced temperature rise and of the aerodynamic quenching are in the order of $\Delta t \approx O(10^{-5}s)$.

The flow accelerates through the first nozzle (3) and reaches the design pre-shock Mach

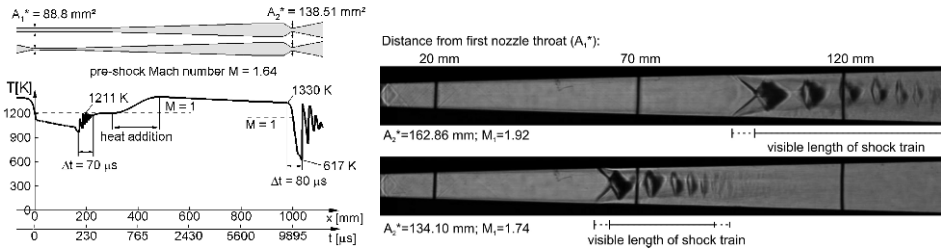


**Fig. 2.** (**a**) Static temperature distribution along axis - left, 3-D Navier-Stokes simulation (SST-model) supersonic reactor, wall cooling, prescribed heat addition, $Q = \frac{q}{c_p T_{01}} = 0.181$, $T_{01} = 1400\,K$, $p_{01} = 10\,bar$, $p_{exit} = 1.3\,bar$ (**b**) Schlieren pictures of the shock system in the first nozzle for different second throat cross sectional areas - right, experiment at low temperature condition, $T_{01} = 292\ K$, $p_{01} = 4.786\ bar$

number of $M = 1.64$. A well defined sudden temperature rise that leads to instantaneous ignition and precursor decomposition would be achieved by a single normal shock (4). In the actual setup the turbulent boundary layer ahead of the shock is relatively thick

and causes substantial shock/boundary layer interactions. Therefore, the single shock disintegrates into a so called pseudo-shock system; i.e., into a sequence of periodic compression and expansion regions [2], Fig. 2b. The shock system length is depending on the pre-shock Mach number. A pre-shock Mach number change from $M = 1.92$ to $M = 1.74$ results in a decreased shock system length as can be seen in Fig. 2b. Such a shock system leads to a final Mach number immediately downstream of the shock train close to $M = 1$. In order to get closer to the result of a normal shock it is planned to apply active and passive control techniques in the area of the shock boundary/layer interaction. To validate the numerical results prior to the realization of the pilot facility, experiments with non-reactive gases at low temperatures were performed. Figure 3 shows the comparison of 3-D numerically and experimentally obtained static pressure distributions on the side wall (a) as well as experimental and numerical Schlieren pictures of the shock structures and locations (b).

The reaction is modeled by three separately treated parts. The primary reaction is the

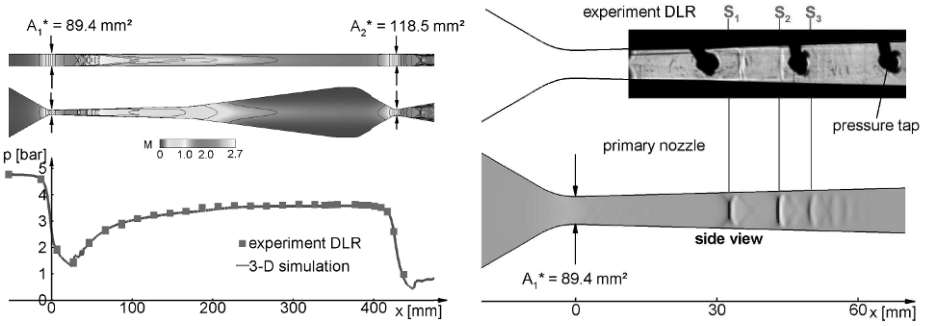


**Fig. 3.** (**a**) Static pressure distribution on sidewall - left (**b**) numerical/experimental Schlieren picture - right $T_{01} = 292\,K$, $p_{01} = 4.786\,bar$, $p_{exit} = 1.3\,bar$, pre-shock Mach number $M = 1.55$, air, dark areas on Schlieren picture due to pressure tabs on sidewall

decomposition of the precursor and the production of monomers. It is modeled by a one step reaction described by an Arrhenius equation. The secondary reaction, the formation of critical nuclei is modeled by classical nucleation theory (CNT). The tertiary reaction is the particle growth by surface condensation, coagulation and single-aggregation. To simulate the particle growth a local polydisperse, unimodal formulation based on the method of moments is used [3]. This method describes the local particle size distribution caused by turbulent mixing and the coagulation.

## 3 Investigation of Precursor Injection and Mixing

Rapid mixing of the precursor with the surrounding hot gas flow is crucial to ensure a homogenous mixture of the reactants and to prevent pre-reactions before entering the shock wave region. For this purpose new injectors are developed and tested in a supersonic wind tunnel, to determine the required injector design and mixing length. Additionally Large Eddy Simulation (LES) is used to analyse the mixing process of the precursor with the hot gas flow. The precursor is injected to the subsonic region ahead of the throat of a convergent-divergent Laval nozzle through a series of holes at the trailing edge of the injector. The injection concept is based on a large velocity difference between the hot

gas flow and the injected precursor flow, to generate a strong shear layer and thereby enhance the mixing process. All different types of injectors tested were designed to work in optimal conditions at an injection Mach number of the surrounding flow of M = 0.6. Laser-induced fluorescence (LIF) imaging is used for visualization of the mixing process. This method allows in-situ observation without influencing the process [4]. For the present experiments toluene, a well-studied fluorescent tracer, diluted in nitrogen is used as a substitute of the precursor. The beam of a frequency-quadrupled Nd:YAG laser (266 nm) is formed to a light sheet (0.5 mm thick, 25 mm wide) and passed the flow channel from bottom to top at various positions. An intensified CCD camera is used to record the fluorescence signal. An exemplar experiment of several investigations is shown in Fig. 4a. In this particular experiment the mass flow of the main air stream is 440 g/s. A mass flow of 0.583 g/s toluene diluted in nitrogen 10 l/min is injected at $M = 0.7$. Downstream of the injector a strong LIF signal can be observed. It decreases with increasing distance to the injection because of dilution with air and quenching by oxygen.

The mixing process of the precursor with the hot gas flow is simulated by LES, since so-

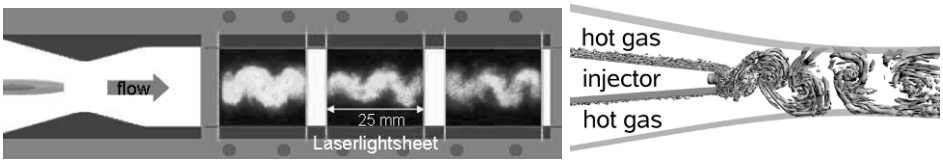


**Fig. 4.** (**a**) Visualisation of TEOS injection and mixing process by means of LIF - left (**b**) vortex contours from LES colour coded with the pressure - right

lutions based on the Reynolds averaged Navier-Stokes equations cannot predict the wake flow field of the injector with strong embedded vortices with sufficient accuracy. Figure 4b shows the vortex structure for a local Mach number of $M = 0.66$ at the trailing edge of the injector. From the simulation results the relation between mixture homogeneity and geometric parameters like nozzle and injector configuration as well as fluid mechanical parameters such as velocitiy ratio (hot gas flow over injector flow), density ratio, mass-flux ratio and angular momentum can be determined. Different approaches to enhance the mixing performance like vortex generators to create longitudinal vortices and inclined injection jets will be considered and also investigated in experiments. The comparison of experimental results and numerical simulations will be used for mutual validation.

## 4 Precursor Decomposition, Particle Growth and Measurement

The ignition delay times of tetraethoxysilane (TEOS) are measured in a shock tube of 80 mm internal diameter with a driver section length of 3.8 m and a length of the driven section of 7.2 m. The driver section is filled with helium and an aluminum diaphragm is deployed to achieve the desired pressure difference. Ignition delay times of TEOS mixtures (1 mass percent TEOS in synthetic air) are measured by monitoring the chemiluminescence CH*-signal near 431 nm for frozen post-shock temperatures ranging from 1150 to 1350 K at an average pressure of 8 bar. Both pressure and CH*-emission histories are obtained from a sidewall measurement to determine the ignition delay time. The results of these experiments are depicted as an Arrhenius representation in Fig. 5a showing that the presence of moisture in the mixture increases the ignition delay times of TEOS. Equations to calculate the ignition delay times $\tau$ are obtained and are also presented in the figure.

An important aspect of the production of $SiO_2$ nanoparticles is the characterization of the product. Small-angle X-ray scattering (SAXS) is a powerful technique to characterize particles in the expected size. A single online measurement is sufficient to determine particle size, size distribution, specific area and fractal dimension simultaneously [5]. The used SAXS camera is based on a development of Kratky [6]. With respect to the distinct design of the shock-wave reactor the camera body is splitted to integrate the reaction chamber into the measurement section and to operate the camera while the production of particles is running. Therefore, two major changes are made. A multilayer X-ray mirror (Göbel mirror), which collimates the divergent X-rays into a parallel and monochromatic beam with high brilliance, is established inside the camera and the one-dimensional, gas-filled detector is replaced by a two-dimensional imaging plate detector. Owing to these changes intensity and image quality are increased. Also the solid-state detector can provide higher counting rates and exhibits an efficiency three times as high as the gas-filled detector which leads to a significantly reduced measurement time.
To characterize particles offline a particle sample is extracted from the reaction chamber by a water-cooled probe. It possesses an outside diameter of 7 mm and is composed of four capillaries (Fig. 5b). Nitrogen is used to dilute the sample at the entrance of the probe. Thus, fast quenching of the sample is possible and chemical reactions as well as particle coagulation are stopped immediately [7]. For investigation purposes the particles are separated on a depth filter that can additionally be equipped with a TEM-grid for further analysis.

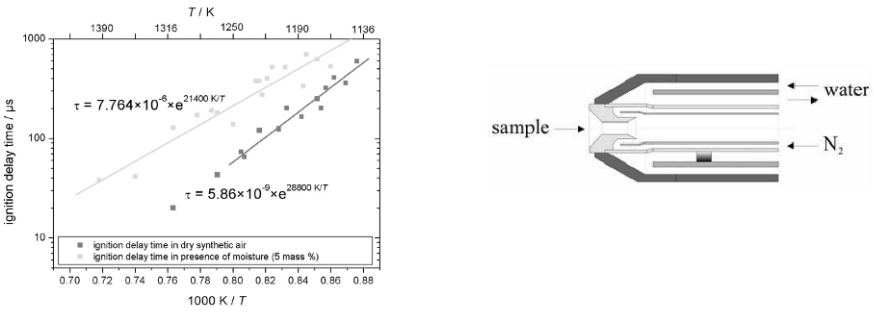


**Fig. 5.** (**a**) Ignition delay times $\tau$ of tetraethoxysilane mixture in dry air (red) and in presence of moisture (green) - left. $[H_2O] = 5$ percent per mass. (**b**) Schematic representation of the sampling probe - right

## 5 Gasdynamic and Evaporative Quenching

Downstream the reaction chamber particle growth is terminated by the cooling effect of a rapid gasdynamic expansion, thereby accelerating the flow up to a Mach number of 2.5. Subsequently to the gasdynamic cooling the specific enthalpy of the gas stream is reduced by evaporation of injected water. Depending on the gas temperature at the inlet of the second nozzle, a mass flow rate of cooling water between 24.2 and 36.1 g/s is required to prevent exceeding the working temperature of the following exhaust system. Figure 6a shows a basic sketch of the quenching system. The cooling water is fed into the gas stream by injection nozzles, which are distributed on the circumference of a slender

cone placed at the nozzle center line and on the surrounding wall to cover the entire cross section. The inlet pressure varies between 8 and 11 bar. At the injection point of the water jets a normal shock is formed which turns into an oblique shock downstream. High relative velocities between gas flow and water disperses the jet into fragments in the order of $10^{-5}$ m and smaller. A large specific phase interface is created to enhance water evaporation. Thus evaporation directly counteracts the temperature rise due to the shock system. An experimental Schlieren image of water injection into a supersonic gas flow is shown in Fig. 6b. At the position of the injection the local Mach number is about 2.3. Because in this case the gas is only preheated up to 320 K, this flow does not include water evaporation.

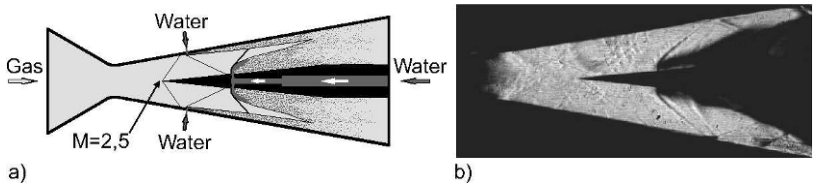


**Fig. 6.** (**a**) Basic sketch of the quenching system - left (**b**) Schlieren-image of water injection into a supersonic gas flow - right

## 6 Conclusion und Outlook

A concept for a new shock-wave reactor for producing nanoparticles starting from the gas-phase is presented. Preliminary studies of the gasdynamic behavior of the shock system, the precursor mixing and the water injection have been carried out numerically and in experiment. The gained knowledge is utilized to design and build up a pilot facility which in the near future will be used for experimental studies, including the generation of nanoparticles.

## References

1. Schild, A., Gutsch, A., Mühlenweg, H., Pratsinis, S.E., "Simulation of nanoparticle production in premixed aerosol flow reactors by interfacing fluid mechanics and particle dynamics", J. Nanoparticles Res. 1, 305-315, (1999)
2. Matsuo, K., Miyazato, Y., Kim, H.D., "Shock train and pseudo-shock phenomena in internal gas flows", Progress in Aerospace Sciences 35, 33-100, (1999)
3. Friedlander, S.K., "Smoke, Dust and Haze. Fundamentals of aerosol dynamics",Oxford University Press, Oxford, New York (2000)
4. C. Schulz, V. Sick, "Tracer-LIF diagnostics: Quantitative measurement of fuel concentration, temperature and air/fuel ratio in practical combustion situations", Prog. Energy Combust. Sci 31, 75-121 (2005)
5. G. Beaucage, H.K. Kammler, S. Pratsinis, "Particle size distribution from small-angle scattering using global scattering functions", Aplied Crystallography, 37, 523, (2004)
6. O. Kratky, "Neues Verfahren zur Herstellung von blendenstreuungsfreien Röntgenkleinwinkelaufnahmen", Z. Elektrochem. 58, 49, 53, (1954)
7. H.K. Ciezki, B. Schwein, "Investigation of gaseous and solid reaction products in a Stepp combustor using a water-cooled sampling probe", AIAA-paper 96-2768, (1996)